CFD/CSD INVESTIGATION OF BVI NOISE REDUCTION USING HARMONIC ACTIVE TWIST CONTROL

David E. Fogarty
david.fogarty@nianet.org
National Institute of Aerospace
100 Exploration Way
Hampton, VA 23666, USA

Matthew L. Wilbur
matthew.l.wilbur@us.army.mil
U. S. Army Research Laboratory Vehicle Technology Directorate

Martin K. Sekula
martin.k.sekula@nasa.gov
Aeroelasticity Branch

D. Douglas Boyd, Jr.
david.d.boyd@nasa.gov
Aeroacoustics Branch

NASA Langley Research Center, Hampton, VA 23681, USA

ABSTRACT

Numerical predictions of the acoustic characteristics of an Active Twist Rotor (ATR) using a loosely coupled Computational Fluid Dynamics (CFD)/Computational Structural Dynamics (CSD) method are presented. The method utilizes the CFD code OVERFLOW2 to compute the rotor blade aerodynamics and the comprehensive code CAMRAD II to predict the elastic blade motion for the ATR. The resulting aerodynamics and blade motion results from this method are then used in the acoustics code PSU-WOPWOP to predict acoustic pressures on a horizontal flat plane of observers located 1.1 rotor diameters beneath the rotor. The distribution of acoustic pressure on the observer plane is used to compute the blade-vortex interaction sound pressure level (BVISPL) representing baseline and actuated conditions. This CFD/CSD method was validated in previous work, and is not used to examine the influence of active twist upon BVI noise reduction. This paper examines a single flight condition of a helicopter in descending flight. The results identify three primary sets of active-twist control inputs which result in the largest decrease in the maximum BVISPL on the observer plane relative to the baseline maximum. Further analysis indicates that the reductions in BVI noise on the observer plane are due to a number of factors – modified rotor disk airloads, changes in the orientation of the vortex relative to the rotor blades, the rate at which the wake is convected away from the rotor, and the induced velocity – all of which have been modified as a result of using active-twist control.

1. INTRODUCTION

Blade-vortex interaction (BVI) noise is a topic of great interest throughout the rotorcraft community, and has been for many years. This type of noise is a result of the interaction of a helicopter rotor blade with the blade tip vortices produced by preceding blades. These interactions generate pressure fluctuations on the surface of the interacting blade which radiate toward the ground as noise. BVI noise occurs primarily in low-speed descending flight, such as landing approach conditions. The frequency content of this type of noise occurs in a range which is audible to the human ear and is considered a significant impediment to the acceptance of rotorcraft by the public. BVI noise is also of critical importance in military operations since mitigating high levels of BVI noise may enhance the effectiveness of helicopters and provide tactical advantages. BVI noise occurs on both the advancing and retreating sides of the rotor. Generally, the advancing side BVI acoustic signal propagates downward and ahead of the rotor. Simultaneously, retreating side BVI noise radiates in a downward direction aft of the rotor, but is generally lower in magnitude compared to the advancing side BVI noise[1].

The characteristics of rotor BVI noise, based on the results of experimental work from both wind-tunnel tests[2-4] and flight test measurements[5-7], have been well documented in the literature. Extensive research has been conducted in both academia and industry in an effort to reduce BVI noise levels of rotorcraft. Passive methods[8-15] generally include variations of blade tip sweep and tip taper, and these alternative blade tip designs have been shown to be effective at reducing BVI noise levels. In addition to passive efforts, numerous active blade control techniques have been developed in an effort to reduce rotorcraft BVI noise. Some examples of these techniques are Higher Harmonic Control (HHC)[16,17], where swashplate actuators excite the blade pitch angle at higher harmonic frequencies of some combination of (N-1), N, and (N+1) per rev where N is the number of blades; active twist control[18,19], where the blade is twisted using active fiber composite actuators embedded within the blade structure; active flap control[20-24]; and Individual Blade Control (IBC)[25-27], where the pitch of each blade is independently controlled in the rotating frame. Both experimental and computational studies examining these techniques have shown that they can be effective in reducing BVI noise.

The current work is an analysis of one of the aforementioned techniques, active-twist control, examining its effect on BVI noise. This analysis utilizes a loosely coupled Computational Fluid Dynamics (CFD)/Computational Structural Dynamics (CSD)

prediction method. This CFD/CSD method has been used extensively[28-33] to predict BVI noise generation in rotorcraft. As a final step in the analysis, results from the CFD/CDS codes are processed by an aeroacoustic analysis code to generate BVI noise predictions.

This paper employs a CFD/CSD method to examine the effect of harmonic active-twist control on BVI noise for the NASA/Army/MIT Active Twist Rotor (ATR)[34]. This method has previously been validated by the authors against experimental measurements[35]. The objective of this paper is to elaborate on and explain the results attained using the CFD/CSD method. To achieve this objective, the authors have chosen a single flight condition (advance ratio 0.17, shaft angle +4°) as the focus of this work.

2. DESCRIPTION OF ATR BLADES

The ATR is a 4-bladed articulated rotor. Each blade has a nominally rectangular planform with a tapered root region, presented in figure 1(a), and a NACA 0012 airfoil section. Active twist is achieved through the use of 24 active fiber composite (AFC) actuators embedded directly in the structure of each blade D-spar. The actuators are placed in four layers through the thickness of the blade and are oriented such that active strain is applied at ±45° relative to the blade's spanwise axis to generate maximum torsional control of the blades. Figure 1(b) illustrates the active-twist concept.

3. DESCRIPTION OF ANALYSIS CODES

3.1 CFD/CSD Analysis

The CFD code used in this study is the Reynolds-Averaged Navier Stokes computational fluid dynamics code OVERFLOW2[36] (version 2.2c). In this code, the solution is calculated using structured overset grids consisting of body-conforming near-body grids and Cartesian off-body grids. The off-body grids are primarily used for modeling the far field wake geometry and extend into the far field a distance of approximately 20 rotor radii to model the rotor wake. The rotor blades are each surrounded by multiple near-body grids capable of modeling blade surface viscous effects. Each ATR blade grid consists of three separate grids – a grid cap at the blade root, a grid cap at the blade tip, and a blade grid in between the root and the tip – as presented in figure 2. Each blade near-body grid extends outward in a direction normal to the blade surface a distance of approximately 1.5 blade chords. As the near-body grids rotate and pass through the off-body grids, hole cutting is required and implemented using an x-ray technique[37]. A loose coupling approach is employed to transfer data between the CFD and CSD analyses. Data is exchanged between the two codes on a quarter revolution basis. As the solution progresses, the airloads from CAMRAD II are gradually replaced with airloads from OVERFLOW2. As outlined in reference 32, at the end of the iterative cycle an additional OVERFLOW2 revolution is executed using the converged elastic blade motion from the final CAMRAD II iteration.

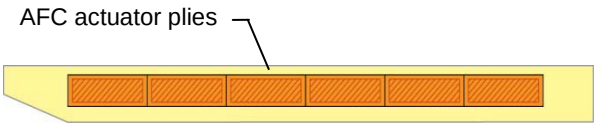

Figure 1(a) Planform of ATR blade.

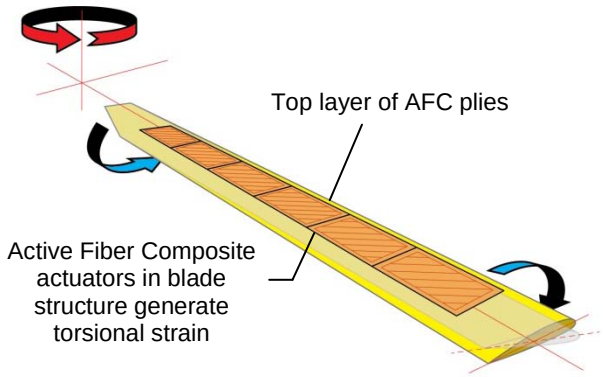

Figure 1(b) Active-twist concept showing root and tip torsional moments and direction of blade rotation.

The second generation version of the Comprehensive Analytical Model of Rotorcraft Aerodynamics and Dynamics (CAMRAD II) code[38] (version 4.7) was used in the present study to model the aeroelastic behavior of the ATR. Active-twist actuation was modeled by imposing a torsional couple on the blade structural model because CAMRAD II does not include a strain induced actuator model. Further discussion on this approach is presented in reference 39. The model was trimmed to a nominal thrust coefficient, C_T, of 0.0066, and the first-harmonic blade flapping with respect to the rotor shaft was trimmed to within 0.1° (to represent wind tunnel trim). Active-twist inputs utilized in this analysis consist of harmonic actuation frequencies of 3P, 4P, and 5P, control phase angles ranging from 0° to 360° (in 30° increments), and an actuation voltage of 1000V. The active twist control function is defined as

$$V=A\cdot\cos(N\psi-\phi)$$

Where A is the amplitude of the control signal, N is the harmonic of actuation, ψ is the azimuth angle, and ϕ is the control phase.

The solution convergence for each CFD/CSD case can be assessed by observing the behavior of the non-dimensional rotor airloads, C_NM^2, at given radial locations on the blade span as a function of azimuth for subsequent coupled iterations. Figure 3 illustrates that approximately 16 coupled iterations are sufficient to reach a converged solution. The solution convergence can be further verified by monitoring the three trim variables, (collective pitch, longitudinal cyclic, and lateral cyclic) and the trim target, C_T. Figures 4 and 5 further substantiate that a converged solution has been reached at approximately 16 coupled trim iterations.

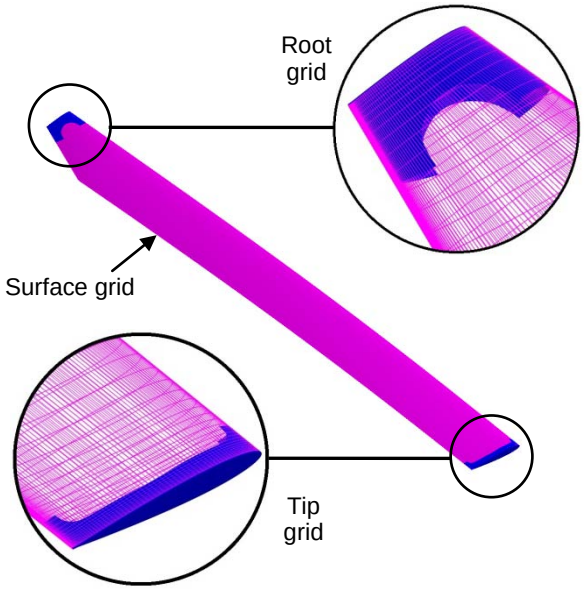

Figure 2 Sample ATR Blade surface grid with insets showing root and tip grids.

3.2 Acoustics Analysis: PSU-WOPWOP

The Ffowcs Williams-Hawkings equation solver, PSU-WOPWOP[40,41], is used to predict rotor discrete-frequency noise using surface pressures and blade motion from the coupled CFD/CSD solution. PSU-WOPWOP computes acoustic pressure time histories at user-defined observer locations. From these acoustic pressure time histories acoustic spectra are then computed at each observer location and integrated over a specific frequency range to obtain an acoustic metric – blade-vortex interaction sound pressure level (BVISPL). It is important to note that the acoustic analysis performed for this paper examined only an isolated rotor. Fuselage effects are not included in the present analysis.

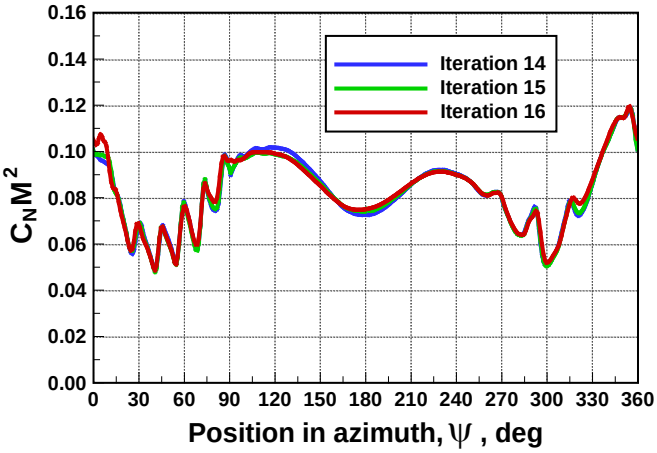

Figure 3 Convergence of rotor airloads, C_NM^2, at a radial location of 0.70R for the baseline case, α = +4.0°, μ = 0.17.

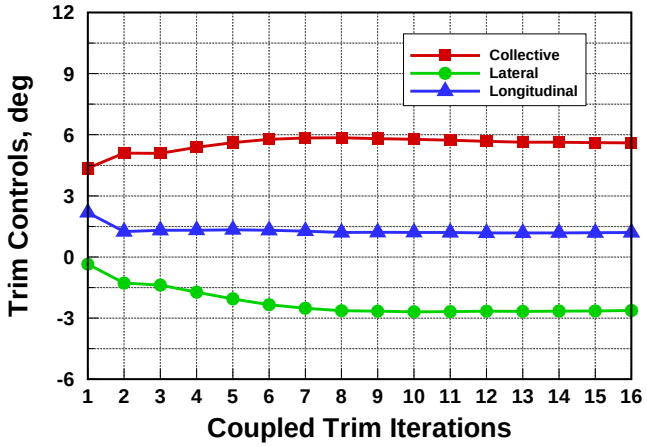

Figure 4 Coupled trim iteration history for trim controls, baseline case, α = +4.0°, μ = 0.17.

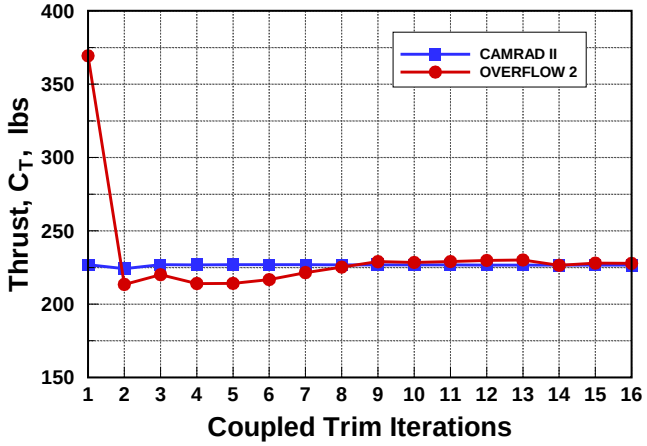

Figure 5 Coupled trim iteration history for trim target, C_T, baseline case, α = +4.0°, μ = 0.17.

Figure 6 presents color contours of BVISPL, for the ATR baseline (active-twist off) case, based on computations by PSU-WOPWOP for a plane of observers located 1.1 rotor diameters beneath the rotor. The location of the ATR rotor disk is represented by the large black circle in the center of the plot and azimuthal positions are indicated accordingly. The observer locations are represented by the grid of small circles. Data from the observer locations can be used to develop a color contour plot representing the distribution of BVI noise relative to the rotor. In figure 6, the free stream velocity originates from the top of the figure. The area of highest BVI noise can be identified as the orange region ahead of the rotor disk. This region contains the maximum BVI noise 101.3 dB.

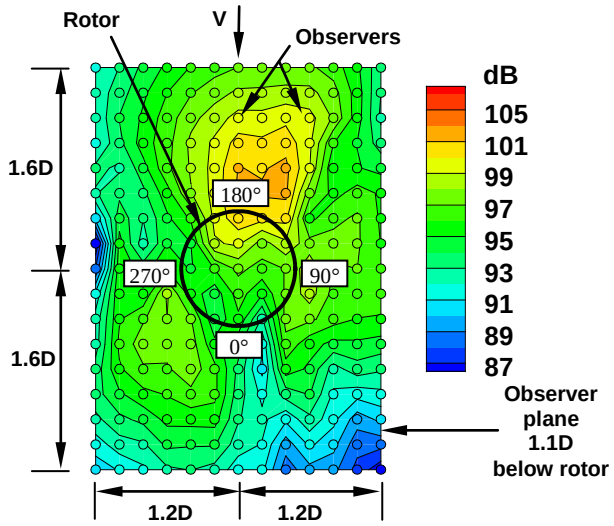

Figure 6 Contours of BVISPL computed using PSU-WOPWOP shown for the ATR baseline case, μ = 0.17 and α=+4°. Top view of observer plane. Observer spacing is 0.2D in each direction on observer plane.

4. RESULTS

4.1 Control Phase Angle

The quantity $BVISPL_{Max}$ is defined as the maximum BVISPL identified on the plane of observers beneath the rotor. This parameter was calculated for each combination of active-twist controls (harmonic actuation frequency and control phase angle) at μ=0.17 and α=+4°.

In this study, an actuation voltage of 1000V is utilized as part of the active twist inputs. It is important to note that while the actuation voltage remains fixed at 1000V, the amount of elastic twist at the blade tip varies as a function of control phase angle for each actuation frequency. For 3P actuation, the elastic twist varies from 1.02° to 1.77°. For 4P and 5P actuation the variation is from 1.45° to 1.82° and from 2.54° to 3.02° respectively.

Figures 7 through 9 show the $BVISPL_{Max}$ as a function of control phase angle, ϕ, for harmonic actuation frequencies of 3P, 4P, and 5P respectively. The horizontal black line in each figure represents the maximum BVISPL, 101.3 dB, for the baseline case. In figures 7 through 9, the red, blue, and green lines represent the CFD predicted results for 3P, 4P, and 5P actuation respectively. For the remainder of this paper, active-twist inputs are represented using the following notation NP/ϕ, where N represents the harmonic actuation frequency per revolution (P), and ϕ represents the control phase angle in degrees. All three figures indicate that the effect of active twist control phase on maximum BVISPL is approximately sinusoidal in nature, regardless of the frequency of actuation. At each actuation frequency, choice of control phase angle is paramount, since active twist can substantially increase BVI noise depending on the control phase angle that is applied.

Figure 7 indicates that, for a 3P actuation frequency, active twist control phase angles ranging from approximately 285° to approximately 120° result in reductions in $BVISPL_{max}$. The maximum reduction occurs at a control phase of 30°, resulting in a 4.0 dB decrease relative to baseline. Conversely, a control phase of 210° corresponds to the largest increase in $BVISPL_{max}$ – 6.8 dB higher than the baseline case.

Figure 8 presents the predicted $BVISPL_{Max}$ using a harmonic actuation frequency of 4P. Control phase angles ranging from 45° to 250° reduce $BVISPL_{max}$ relative to baseline. The minimum $BVISPL_{max}$ value of 97.8 dB occurs at a control phase angle of approximately 120°. This 3.5 dB reduction is an improvement compared to the best 3P actuation case. The maximum BVI noise relative to the baseline occurs at a control phase angle of 300° – a 4.6 dB increase in noise.

Figure 9 presents the $BVISPL_{Max}$ as a function of control phase angle for the baseline case and a 5P harmonic actuation frequency. $BVISPL_{Max}$ is reduced by actuating the rotor using control phase angles ranging from 180° to 360° with maximum $BVISPL_{Max}$ reduction of 4.5 dB occurring at 300° control phase angle. Figure 9 indicates that active twist controls of 5P/300° produce the largest reductions in BVI noise of all the active twist control combinations examined. The largest increase in $BVISPL_{Max}$ occurs at a control phase of 120° resulting in a 4.4 dB increase.

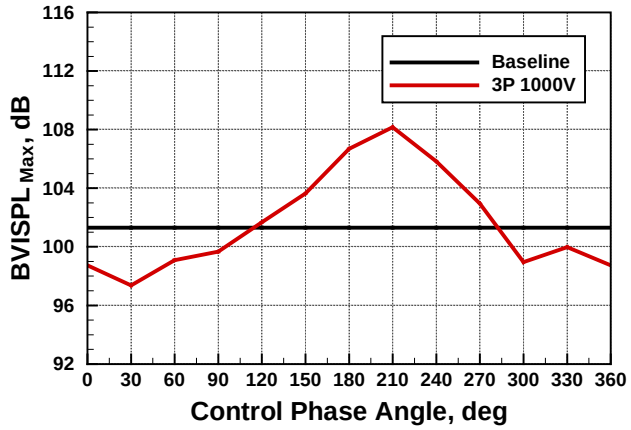

Figure 7 $BVISPL_{Max}$ as a function of active-twist control phase angle using a 3P actuation frequency, μ = 0.17, α = +4°.

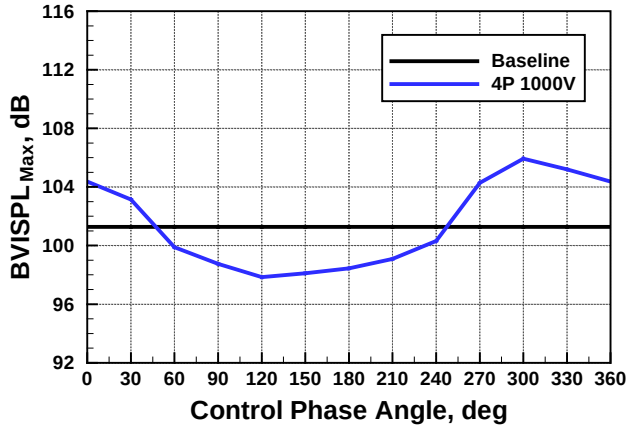

Figure 8 $BVISPL_{Max}$ as a function of active-twist control phase angle using a 4P actuation frequency, μ = 0.17, α = +4°.

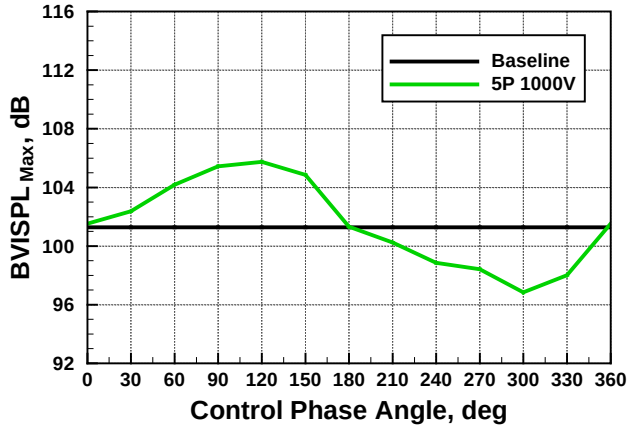

Figure 9 $BVISPL_{Max}$ as a function of active-twist control phase angle using a 5P actuation frequency, μ = 0.17, α = +4°.

4.2 BVISPL Distribution

The following section Figures 10 through 12 presents color contour plots of the distribution of BVISPL for the baseline (unactuated) case to active-twist inputs which increase $BVISPL_{Max}$ and active-twist inputs which decrease $BVISPL_{Max}$. These comparisons for 3P through 5P frequencies of actuation are presented in figures 10 through 12, respectively. The location of the maximum BVISPL, represented by the solid black circle, and magnitude are indicated on each plot.

Figure 10(b) shows that active-twist inputs of 3P/210 degrees substantially increase the maximum BVISPL on the observer plane relative to the baseline. This increase is on the order of 7 dB and is clearly shown on the advancing side of the rotor in the red region, or “hot-spot”. It is also worth noting that this region of high noise has shifted relative to the baseline to a slightly more aft position on the advancing side of the rotor. In complete contrast to this result, figure 10(c) shows the effects of actuating the rotor with 3P/30 degrees active twist controls. Changing the control phase angle has a significant impact on the distribution and magnitude of BVI noise on the observer plane. The region of high noise present in the baseline case has been significantly alleviated and the maximum BVISPL, now occurring directly beneath the rotor, has been reduced in magnitude by approximately 4 dB relative to the baseline. Other significant areas of BVI noise reduction occur forward of the rotor on both the advancing and retreating sides. It is noteworthy that on the retreating side of the rotor there exists a location where the noise is approximately 10 dB lower than the baseline.

Figures 11(b) and 12(b), although resulting from two different sets of active-twist inputs, are quite similar with regards to the directivity of BVI noise on the observer plane. Both plots show an increase in the maximum BVISPL on the order of 4 to 4.5 dB relative to the baseline. Figures 11(c) and 12(c) also show similar characteristics with regions of decreased BVI noise both aft and forward of the rotor. However, figure 12(c) shows that the 5P/300 degree active-twist inputs produce greater reductions relative to the baseline than the 4P/120 degrees. These reductions are evident in two locations – ahead of the rotor on the retreating side in figure 12(c) where there is a large region of reduced noise, and the maximum BVI noise on the observer plane has been reduced by 4.5 dB as opposed to a 3.5 dB reduction in figure 11(c).

4.3 Acoustic Pressure Time Histories

The BVISPL distributions show that decibel levels can be reduced in the BVI frequency range. To provide more detail about the changes that are taking place with the application of active twist, acoustic

pressure time histories for a single rotor revolution are presented in Figures 13 through 15. These pressure time histories were calculated at the observer in the observer plane which measured the maximum value of BVISPL for the baseline case. The location of this observer is indicated in Figure 10(a).

For the 3P active-twist inputs, the acoustic pressure time histories are shown in Figures 13(a) through 13(c). The low frequency loading from all four blades can be seen. In addition, it is clearly seen that the increase in BVISPL seen in Figure 10(b) is caused by an increase in the number and magnitude of the blade vortex interactions. Likewise, the reduction of BVISPL seen in Figure 10(c) is caused by a drastic reduction in the number and strength of the blade vortex interaction events. These changes are consistent with the notion that application of active-twist affects the strength and/or location of the vortex relative to the blade[19].

Similar changes can be seen for the 4P active-twist when comparing Figures 14(a) through (c) with Figures 11(a) through (c) and for the 5P active twist when comparing Figures 15(a) through (c) with Figures 12(a) through (c).

4.4 Airloads

Figures 16 through 18 present the time derivative of the non-dimensional rotor disk airloads, $d(C_N M^2)/dt$. The rotor airloads in figures 16 through 18 correspond to the BVISPL contour plots in figures 10 through 12 respectively.

Two major advancing side BVI interactions, identified by the black ellipses, can be seen in the baseline case in Figure 16(a). These interactions occurring in the first quadrant of the rotor disk exhibit somewhat parallel characteristics and result in the region of high noise ahead of the rotor identified in figure 10(a). There are also several less intense interactions on the retreating side of the rotor disk which are representative of oblique and perpendicular BVI interactions.

The active-twist inputs which increase the noise relative to the baseline – 3P/210, 4P/300, and 5P/120 – are represented in subplots (b) in figures 16 through 18 respectively. These three airloads plots display similar characteristics indicating that there are additional interactions in the first quadrant of the rotor disk. These interactions, although appearing weaker, are parallel in orientation. These interactions are considered the primary contributors to the increases in BVI noise identified in subplots (b) of figures 10 through 12. It is worth noting the presence of additional interactions on the retreating side of the rotor. While these interactions appear higher in magnitude than those on the advancing side, they are more oblique in orientation relative to the rotor blades. Therefore these interactions do not generate as much noise as parallel interactions. These oblique BVI's are considered to be the primary contributors to the increase in noise identified aft of the rotor in subplots (b) of figures 10 through 12.

Similarly, the active-twist inputs which reduce the noise relative to the baseline – 3P/30 degrees, 4P/120 degrees, and 5P/300 degrees – are represented in subplots (c) in figures 16 through 18 respectively. In figure 16(c) the 3P active-twist inputs have changed the interaction angle between the vortex and the blade resulting in several oblique BVI's on the advancing side. In figure 17(c) the intensity of the advancing side BVI's has been reduced and in figure 18(c) the magnitudes of the two advancing side BVI's have intensified relative to the baseline, however their orientation is now more oblique in nature resulting in the decrease in BVI noise shown in the contour plot in figure 12(c).

4.5 Rotor Wake Geometry

The effect of the active-twist inputs on the rotor wake is examined using the wake geometry plots presented in figures 19 through 21. Each figure presents top and oblique views of iso-surfaces of the velocity gradient tensor (the "Q"-criterion). The baseline wake structure is represented in grey and the active-twist wake structure is represented in blue. Red arrows are utilized in the figures to highlight significant differences in the wake structures between the baseline and the active-twist cases. Figures 19 through 21 clearly illustrate that the active-twist, regardless of the harmonic actuation frequency, has a considerable effect on the wake structure. The primary differences between the baseline and the active-twist cases are 1) the rate at which the vortices are convected away from the rotor disk, and 2) the interaction angle between the vortices and the rotor blades. The three figures indicate that employing active-twist controls that minimize BVI noise (3P/30, 4P/120, and 5P/300), increases the vortex induced velocity relative to the baseline resulting in faster convection of the wake below the rotor. Conversely, active-twist controls that increase BVI noise (3P/210, 4P/300, and 5P/120) reduce the induced velocity relative to baseline, thereby resulting in a slower convection of the wake below the rotor.

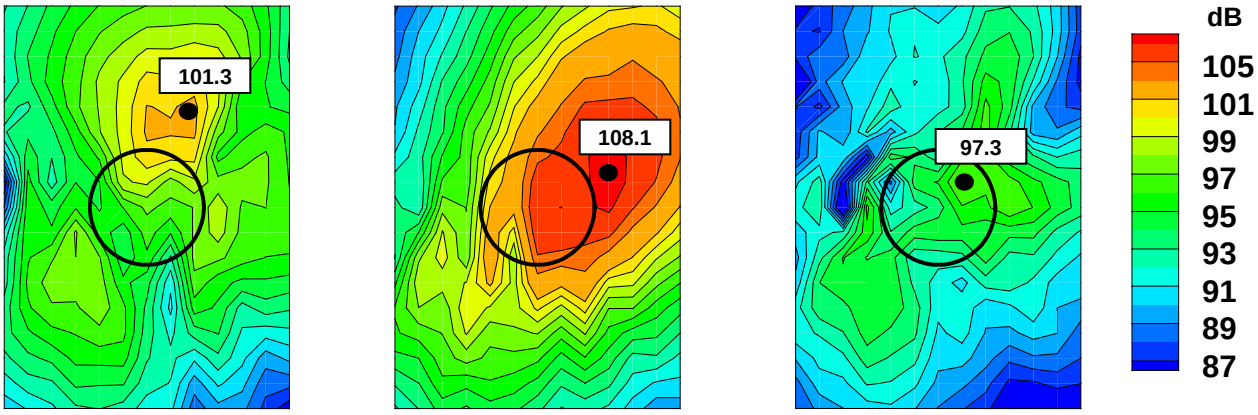

(a) Baseline (active-twist off) (b) Max. noise, 3P/210° (c) Min. noise, 3P/30°

Figure 10 Contours of BVISPL on the observer plane beneath the rotor for the (a) baseline, (b) 3P with a 210° control phase angle, and (c) 3P with a 30° control phase angle, μ = 0.17, α = 4°.

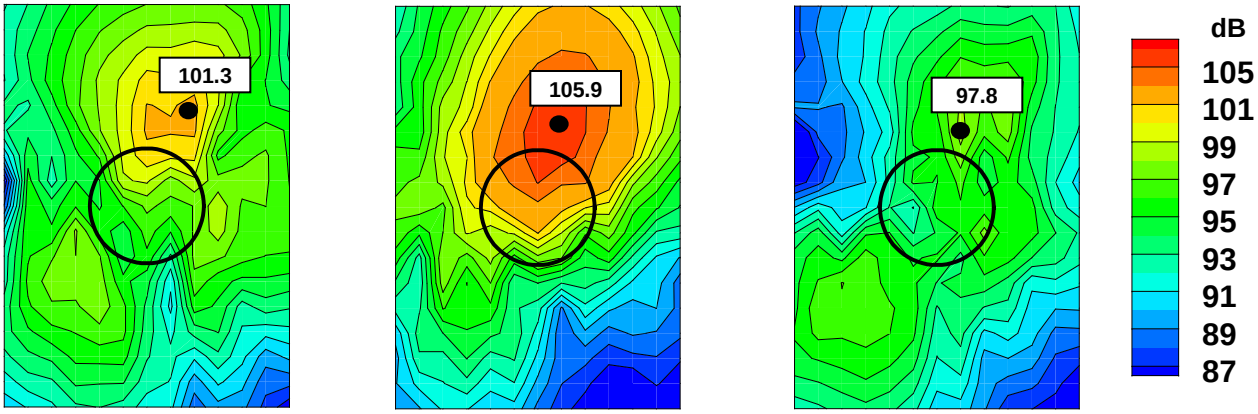

(a) Baseline (active-twist off) (b) Max. noise, 4P/300° (c) Min. noise, 4P/120°

Figure 11 Contours of BVISPL on the observer plane beneath the rotor for the (a) baseline, (b) 4P with a 300° control phase angle, and (c) 4P with a 180° control phase angle, μ = 0.17, α = 4°.

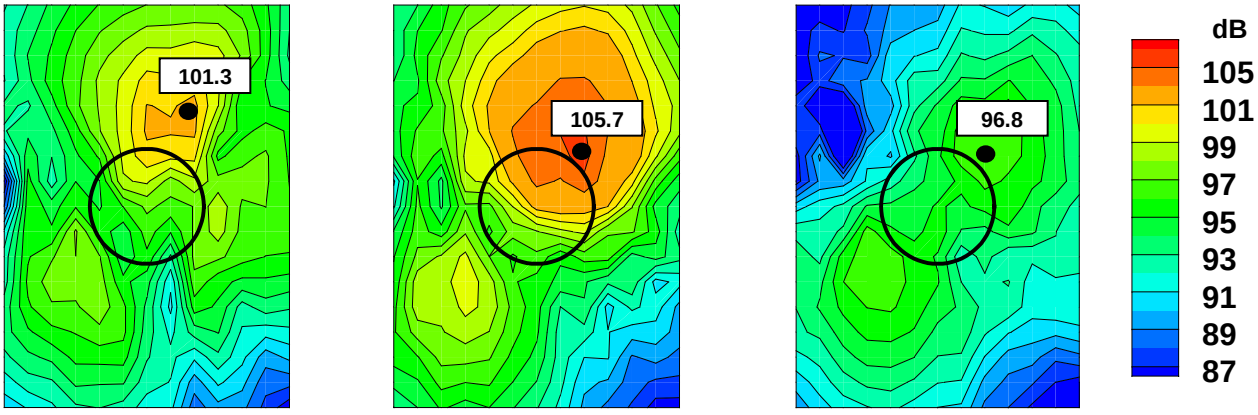

(a) Baseline (active-twist off) (b) Max. noise, 5P/120° (c) Min. noise, 5P/300°

Figure 12 Contours of BVISPL on the observer plane beneath the rotor for the (a) baseline, (b) 5P with a 120° control phase angle, and (c) 5P with a 300° control phase angle, μ = 0.17, α = 4°.

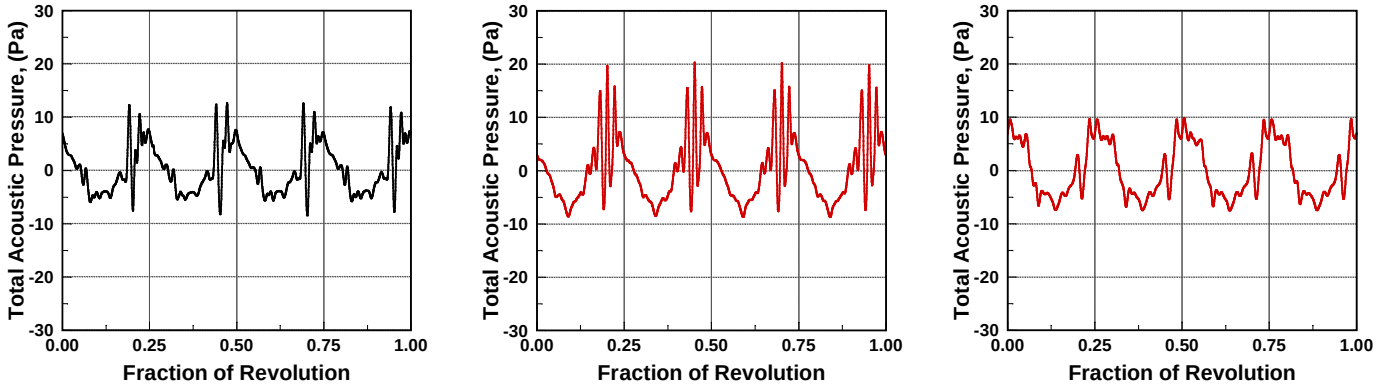

(a) Baseline (active-twist off) (b) 3P/210° (c) 3P/30°

Figure 13 Acoustic pressure-time histories for the baseline BVISPL$_{Max}$ location and the same location on the observer plane for 3P active-twist.

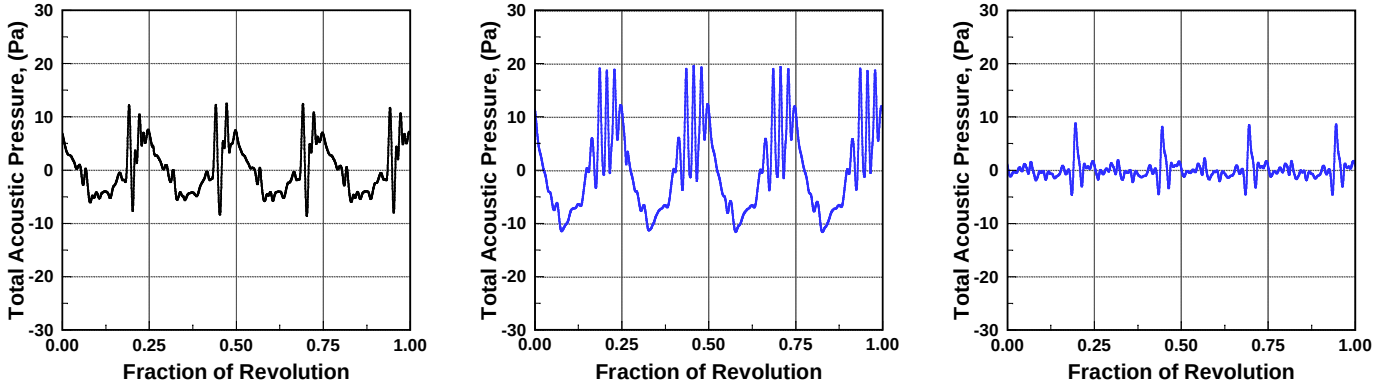

(a) Baseline (active-twist off) (b) 4P/300° (c) 4P/120°

Figure 14 Acoustic pressure-time histories for the baseline BVISPL$_{Max}$ location and the same location on the observer plane for 4P active-twist.

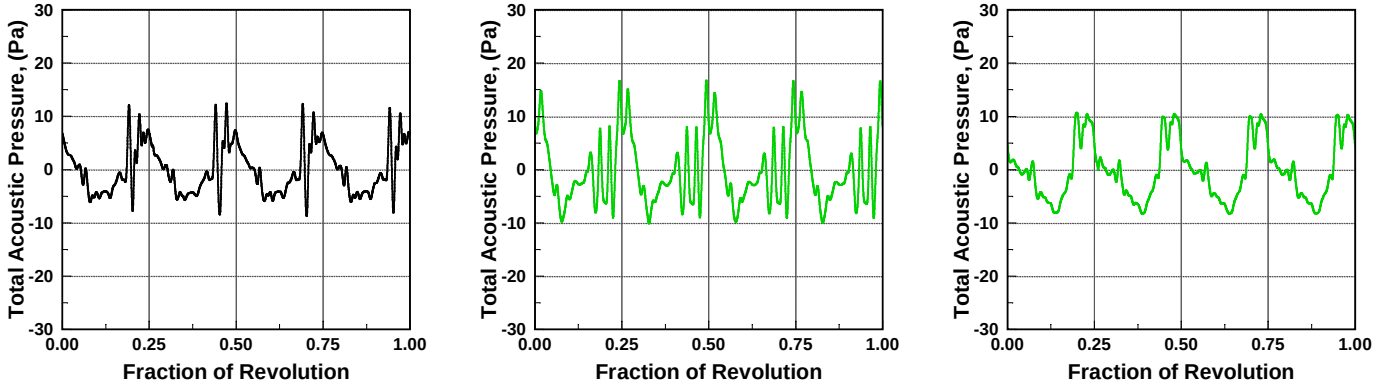

(a) Baseline (active-twist off) (b) 5P/120° (c) 5P/300°

Figure 15 Acoustic pressure-time histories for the baseline BVISPL$_{Max}$ location and the same location on the observer plane for 5P active-twist.

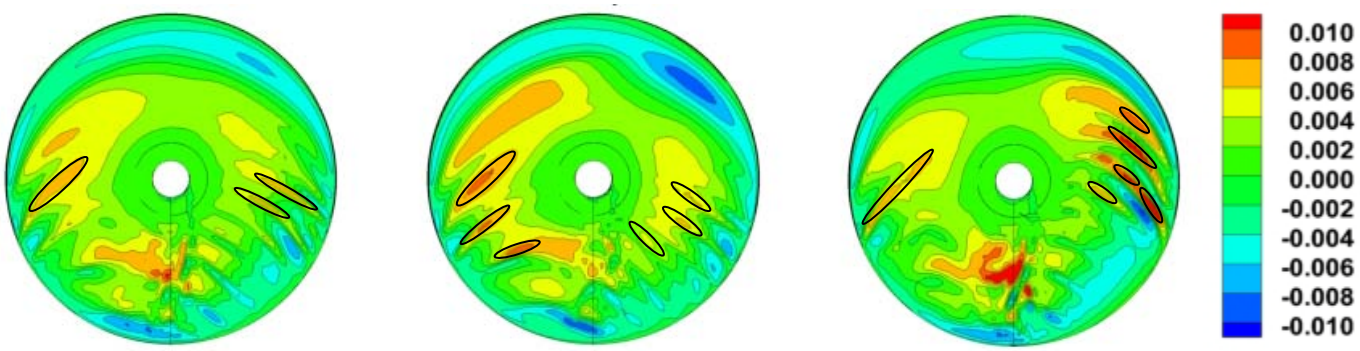

(a) Baseline(active-twist off) (b) Max. noise, 3P/210° (c) Min. noise, 3P/30°

Figure 16 Contours of $d(C_N M^2)/dt$ over the entire rotor disk for the (a) baseline, (b) 3P with a 210° control phase angle, and (c) 3P with a 30° control phase angle, μ=0.17, α=4°.

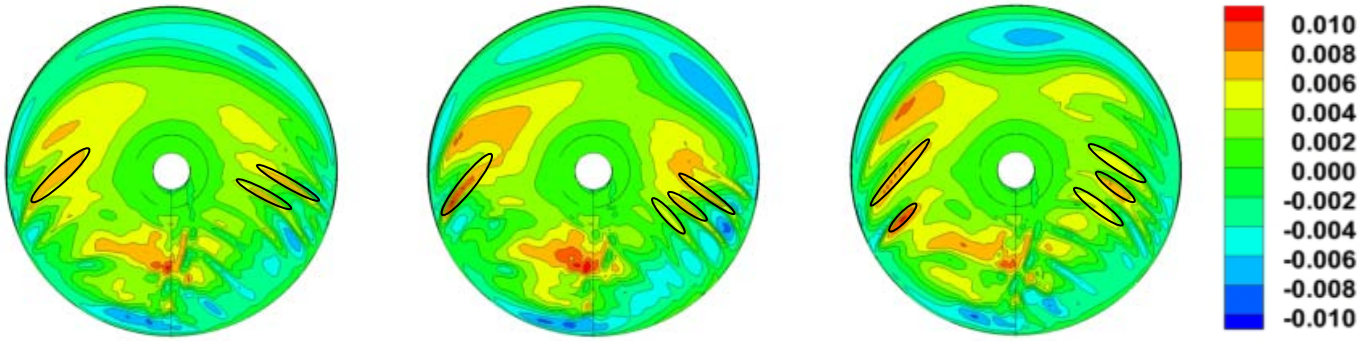

(a) Baseline(active-twist off) (b) Max. noise, 4P/300° (c) Min. noise, 4P/120°

Figure 17 Contours of $d(C_N M^2)/dt$ over the entire rotor disk for the (a) baseline, (b) 4P with a 300° control phase angle, and (c) 4P with a 120° control phase angle, μ=0.17, α=4°.

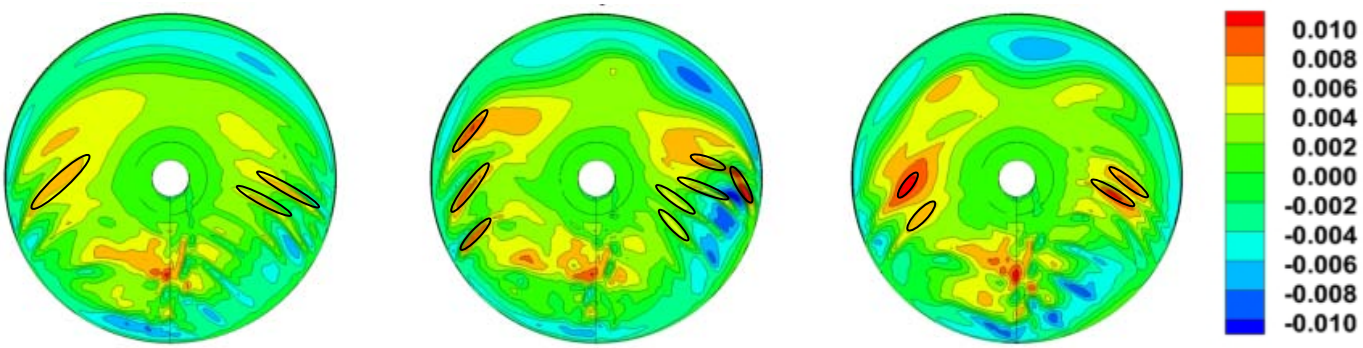

(a) Baseline(active-twist off) (b) Max. noise, 5P/120° (c) Min. noise, 5P/300°

Figure 18 Contours of $d(C_N M^2)/dt$ over the entire rotor disk for the (a) baseline, (b) 5P with a 90° control phase angle, and (c) 5P with a 300° control phase angle, μ=0.17, α=4°.

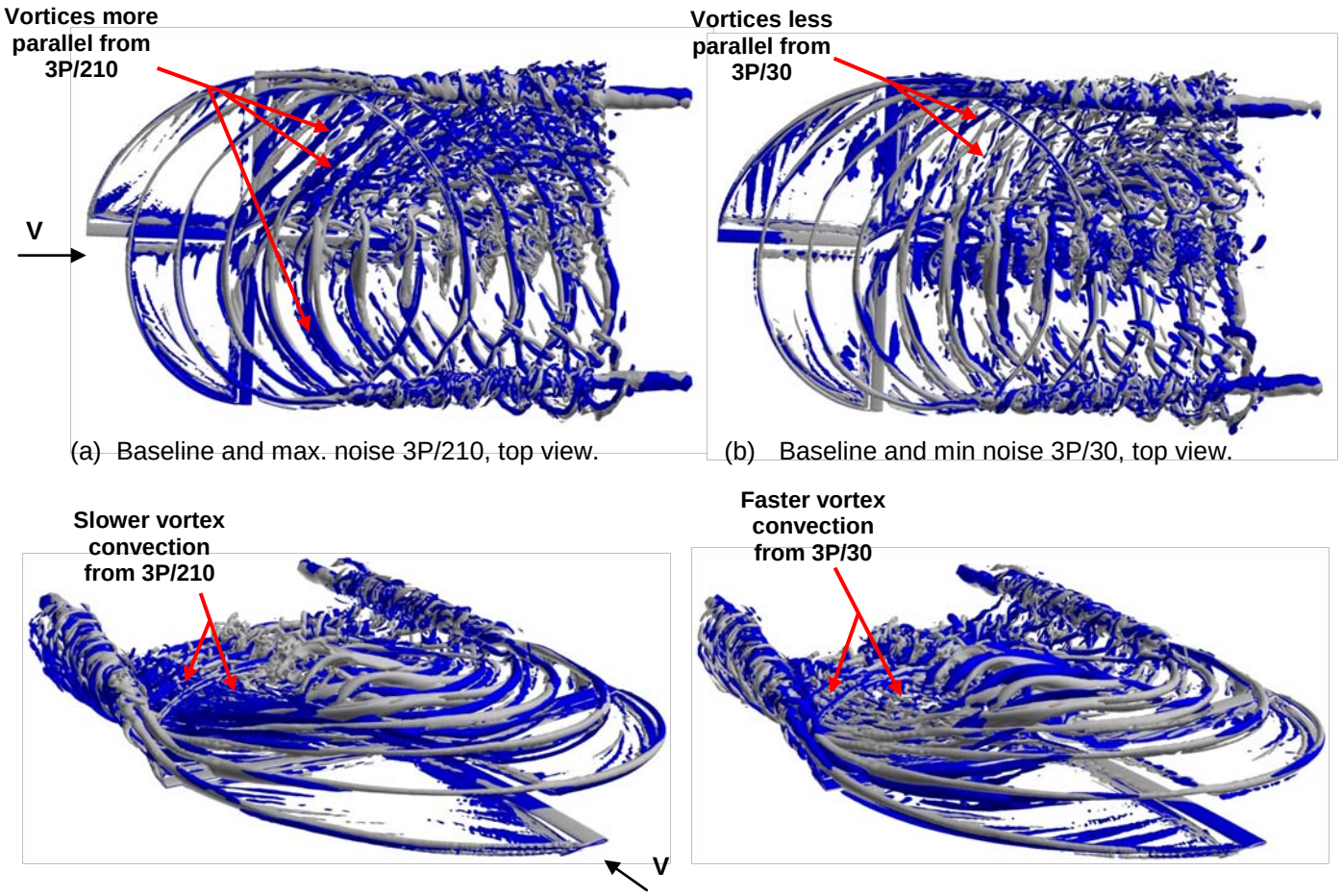

(a) Baseline and max. noise 3P/210, top view.

(b) Baseline and min noise 3P/30, top view.

(c) Baseline and max. noise 3P/210, oblique view.

(d) Baseline and min. noise 3P/30, oblique view.

Figure 19 Wake geometry for baseline, (grey) and 3P active-twist (blue), μ=0.17, α=4°.

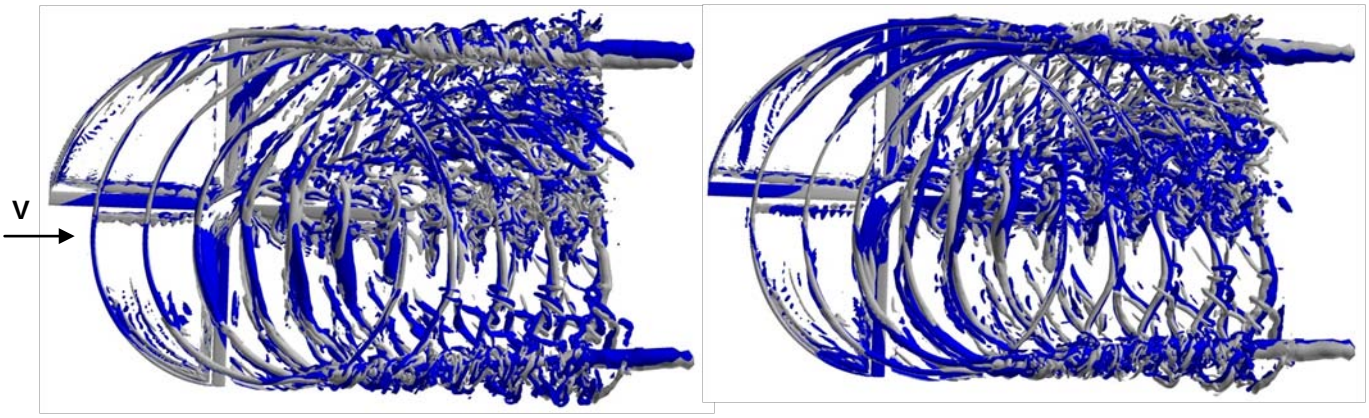

(a) Baseline and max. noise 4P/300, top view.

(b) Baseline and min noise 4P/120, top view.

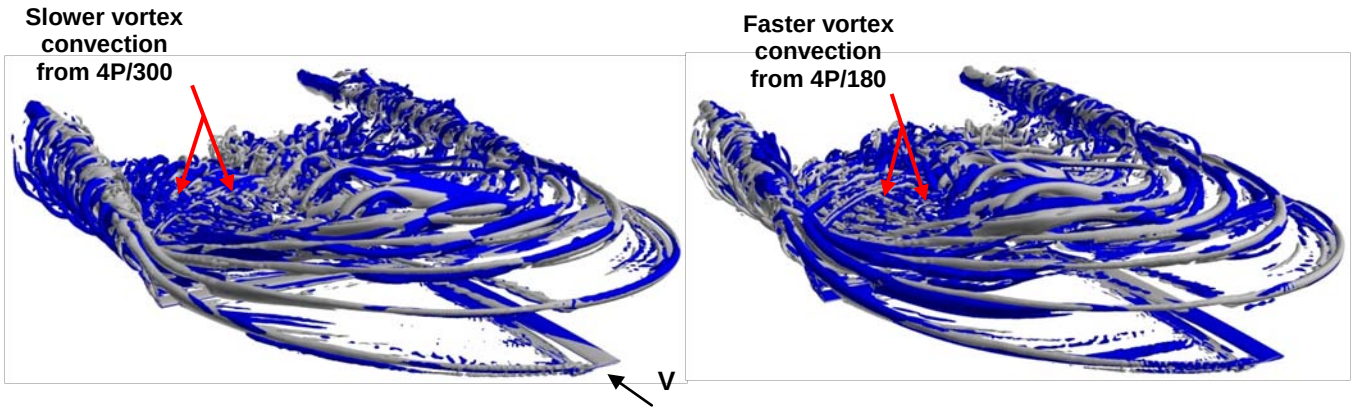

(c) Baseline and max. noise 4P/300, oblique view.

(d) Baseline and min. noise 4P/120, oblique view.

Figure 20 Wake geometry for baseline, (grey) and 4P active-twist (blue), μ=0.17, α=4°.

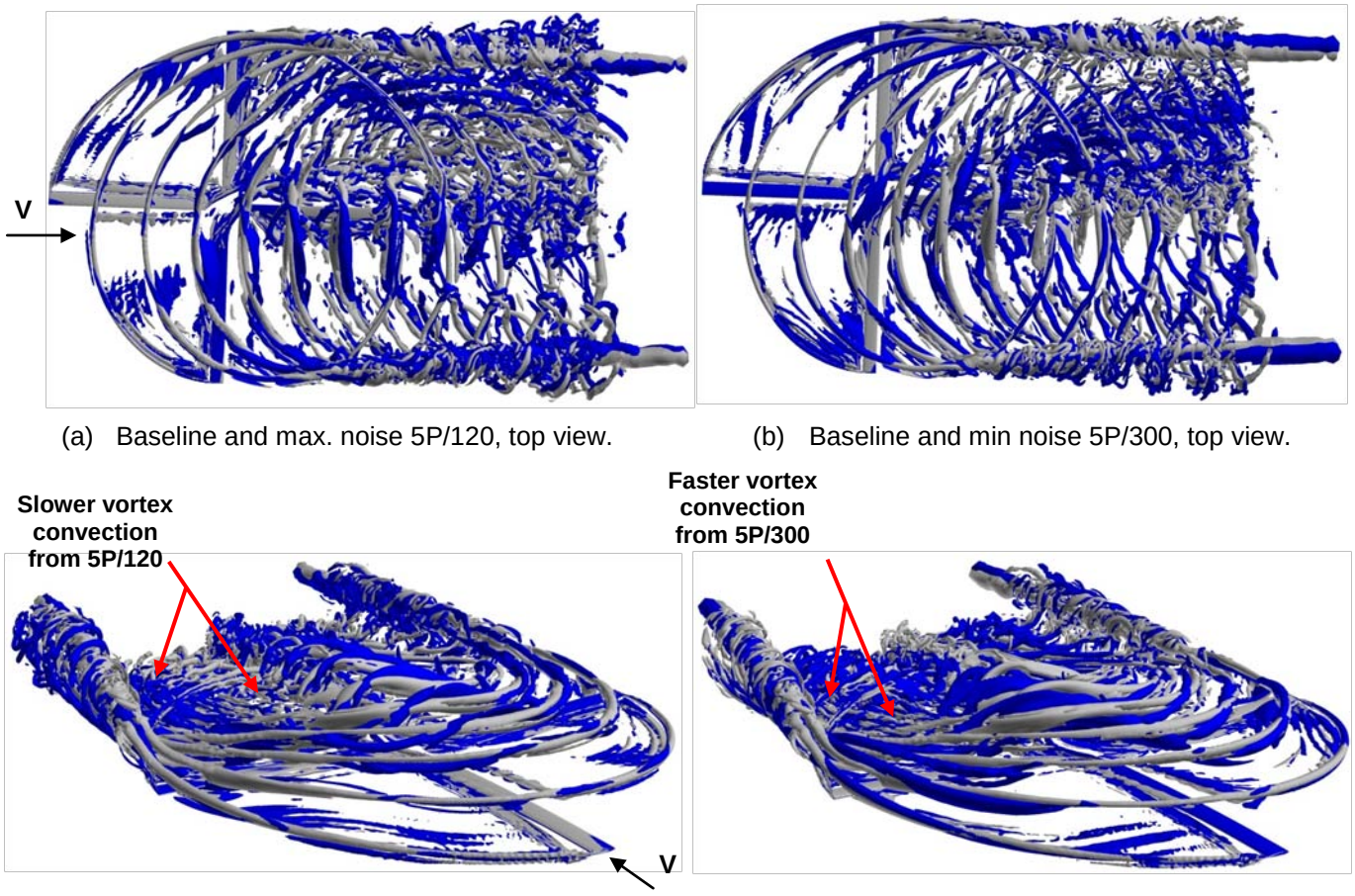

(a) Baseline and max. noise 5P/120, top view.

(b) Baseline and min noise 5P/300, top view.

(c) Baseline and max. noise 5P/120, oblique view.

(d) Baseline and min. noise 5P/300, oblique view.

Figure 21 Wake geometry for baseline, (grey) and 45 active-twist (blue), μ=0.17, α=4°.

4.6 Blade Tip Pitch Response

The source of the advancing side interactions in the first quadrant can be traced to preceding revolutions where the vortices are released by blades in the second quadrant. These vortices are convected downstream and ultimately generate blade-vortex interaction events in the first quadrant [25,26]. Similarly, the BVI events in the fourth quadrant on the retreating side are a result of vortices released in the third quadrant. The strength of the tip vortices is determined by the lift produced by the blade. Figures 22 through 24 present the blade tip pitch as a function of control phase angle for the baseline case which is represented by the black line, and the 3P, 4P, and 5P harmonic actuation frequencies which are represented by the red, blue, and green lines respectively. The active-twist inputs which result in a reduction in noise relative to the baseline are represented by the solid colored line in each figure. The active-twist inputs which result in an increase in noise relative to the baseline are represented by the dashed colored line in each figure. Figure 22 shows an increase of approximately 2.0° in blade tip pitch (relative to the baseline) occurring at an azimuth angle of 135° with the 3P/30° active-twist inputs. This increase in blade tip pitch increases the lift produced by the blade resulting in a stronger tip vortex. The increase in lift and vortex strength produces a new induced velocity field yielding faster rotor wake convection, as discussed in the previous section, (see figures 19(b) and (d), for example) a reduction in BVI rotor airloads and ultimately a decrease in BVI noise. It is also worth noting that the change in blade flap-wise displacement at the blade tip is on the order of one blade thickness and its effect on BVI noise generated is considered negligible. Because these blade flapping changes are small, they do not appear to significantly contribute to the changes in miss-distance between the wake and the blade. For the 3P/210 degrees active-twist inputs, there is a decrease in blade pitch of approximately 2.0°, relative to the baseline at 135° rotor azimuth.

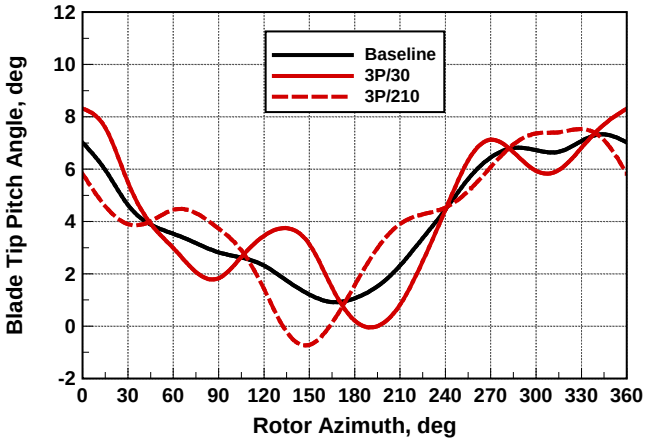

Figure 22 Blade tip pitch angle for baseline and 3P harmonic active-twist actuation, μ=0.17, α=4°.

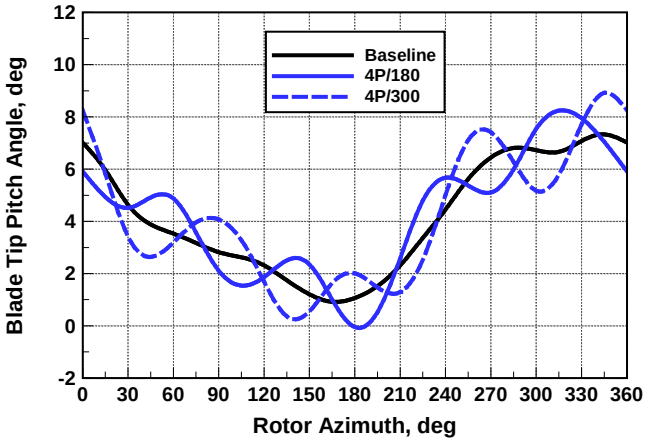

Figure 23 Blade tip pitch angle for baseline and 4P harmonic active-twist actuation, μ=0.17, α=4°.

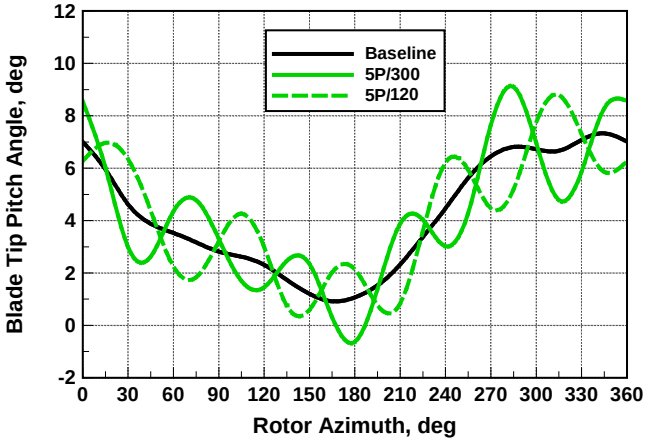

Figure 24 Blade tip pitch angle for baseline and 5P harmonic active-twist actuation, μ=0.17, α=4°.

This decrease in pitch reduces the strength of the tip vortex but consequently reduces the induced velocity resulting in locally slower rotor wake convection, as noted in figures 19(a) and (c). This change in wake convection allows the shed tip vortices to interact with rotor blades for a prolonged period of time hence contributing to the generation of additional BVI events and greater BVI rotor airloads. Similar observations can be made by examining the blade tip pitch response and the wake geometry for 4P and 5P active-twist actuation presented in figures 23 and 20 and figures 21 and 24, respectively.

5. CONCLUSIONS

Numerical predictions of the acoustic characteristics of an Active Twist Rotor (ATR) using a loosely coupled Computational Fluid Dynamics (OVERFLOW2) /Computational Structural Dynamics (CAMRADII) method combined with aeroacoustic analysis PSU-WOPWOP were presented. The analysis concentrated on a single flight condition – advance ratio of 0.17, 4° nose-up pitch. The results of this study indicate:

- Active-twist control modifies the blade pitch which in turn affects the rate at which the wake is convected away from the rotor, the vortex intensity, and the vortex orientation.
- Active-twist actuation, harmonic actuation frequency and control phase angle have a substantial impact on the rotor wake structure.
- The reductions in BVI noise can be attributed to an increase in miss distance and a change in the vortex orientation becoming increasingly more oblique relative to the interacting rotor blade.
- Three sets of 1000V active-twist inputs have been identified which reduce the maximum BVI noise: 1) 3P/30 – reduction of 4.0 dB, 2) 4P/120 – reduction of 3.5 dB, and 3) 5P/300 – reduction of 4.5 dB.
- Not only has active-twist been recognized as reducing the maximum BVISPL on the observer plane, significant reductions, on the order of (10 to 11 dB) in noise were noted to occur, specifically in the region forward of the rotor and also on the retreating side.
- The changes in blade flapping due to the active-twist in the cases examined are on the order of one blade thickness or less and therefore provide a negligible contribution to the miss-distance changes between the wake and blade.

6. REFERENCES

1. Martin, R. M., Splettstoesser, W. R., Elliott, J. W., and Schultz, K. J., “Advancing Side Directivity and Retreating Side Interactions of Model Rotor Blade Vortex Interaction Noise,” NASA TP-2784, May 1988.

2. Splettstoesser, W. R., Schultz, K. J., Boxwell, D. A., and Schmitz, F. H., “Helicopter Model Rotor-Blade Vortex Interaction Impulsive Noise: Scalability and Parametric Variations,” NASA TM-86007, Dec. 1984.

3. Hoad, D. R., “Helicopter Model Scale Results on Blade-Vortex Interaction Impulsive Noise as Affected by Tip Modification,” American Helicopter Society, AHS Paper 80-62, May 1980.

4. Martin, R. M., and Connor, A. B., “Wind Tunnel Acoustic Results of Two Rotor Models with Several Tip Designs,” NASA TM-87698, July 1986.

5. Boxwell, D. A., and Schmitz, F. H., “Full-Scale Measurements of Blade Vortex Interaction Noise,” Journal of the American Helicopter Society, Vol. 27, No. 4, 1982, pp. 11-27.

6. Charles, B. D., “Acoustic Effects of Rotor-Wake Interaction During Low-Power Descent,” American Helicopter Society Symposium on Helicopter Aerodynamic Efficiency, May 1975.

7. Tangler, J. L., “Schlieren and Noise Studies of Rotors in Forward Flight,” American Helicopter Society, AHS Paper 77.33-05, May 1977.

8. Smith, D. E., “Helicopter Rotor Tip Shapes For Reduced Blade-Vortex Interaction - An Experimental Investigation,” AIAA Paper 95-0192, Presented at The Aerospace Sciences Meeting and Exhibit, 33rd, Reno, NV, Jan 9-12, 1995.

9. Mullins, Jr., B. R., Smith, D. E., Rath, C. B., and Thomas, S. L., “Helicopter Rotor Tip Shapes For Reduced Blade-Vortex Interaction - An Experimental Investigation, Part II,” AIAA Paper 96-0149, Presented at The Aerospace Sciences Meeting and Exhibit, 34th, Reno, NV, Jan. 15-18, 1996.

10. Rath, C. B., “Wing Tip Vortex Stagnation Pressure Survey of Various Tip Shapes,” MSAE Thesis, The University of Texas at Arlington, 1991.

11. Mosher, M., “Acoustic Measurements of a Full-Scale Rotor with Four Tip Shapes Vol. I, Text, Appendix A and Appendix B,” NASA TM-85878-VOL-1, April, 1994.

12. Mosher, M., “Acoustic Measurements of a Full-Scale Rotorwith Four Tip Shapes Vol. II, Appendix C, Appendix D, Appendix E and Appendix f,” NASA TM-85878-VOL-2, April, 1994.

13. Hoad, D. R., “Helicopter Blade Slap Noise Variation with Tip Vortex Modification,” Masters Dissertation, George Washington University, Washington, DC. May 1979.

14. Landgrebe, A. J., and Bellinger, E. D., “Experimental Investigation of Model Variable Geometry and Ogee Tip Rotors,” NASA CR-2275, Feb. 1974.

15. Mantay, W. R.; Campbell, R. L.; and Shidler, P. A., “Full Scale Testing of an Ogee Tip Rotor,” NASA CP-2052, 1978, pp. 277-308.

16. Splettstoesser, W.R., Kube, R., Seelhorst, U., Wagner, W., Boutier, A., Micheli, F., Mercker, E., Pengel, K.: “Higher Harmonic Control Aeroacoustic Rotor Test (HART) – Test Documentation and Representative Results,” IB 129-95/28, Deutsche Forschungsanstalt für Luft- und Raumfahrt, December 1995.

17. Brooks, T. F., and Booth, E. R., Jr., “The Effects of Higher Harmonic Control on Blade-Vortex Interaction Noise and Vibration,” Journal of the American Helicopter Society, Vol. 38 (3), July 1993.

18. Fogarty, D. E., Wilbur, M. L., and Sekula, M. K., “A Computational Study of BVI Noise Reduction Using Active Twist Control,” American Helicopter Society 66th Annual Forum and Technology Display, Phoenix, AZ, May 11-13, 2010.

19. Fogarty, D. E., Wilbur, M. L., and Sekula, M. K., “The Effect of Non Harmonic Active Twist Actuation on BVI Noise,” American Helicopter Society 67th Annual Forum and Technology Display, Virginia Beach Convention Center, Virginia Beach, VA, May 3-5, 2011.

20. Patt, D., Liu, L., and Friedmann, P. P., “Simultaneous Vibration and Noise Reduction in Rotorcraft Using Aeroelastic Simulation,” American Helicopter Society 60th Annual Forum, Baltimore, MD, June 7-10, 2004.

21. Patt, D., Liu, L., and Friedmann, P. P., “Rotorcraft Vibration Reduction and Noise Prediction Using a

Unified Aeroelastic Response Simulation," Journal of the American Helicopter Society, Vol. 50 (1), 2005.

22. Baeder, J.D., and Sim, B.W., "Blade Vortex Interaction Noise Reduction by Active Trailing Edge Flaps," Proceedings of the 54th Annual Forum of the American Helicopter Society, 1998.

23. Aoyoma, T., Yang, C., and Saito, S., "Numerical Analysis of Active Flap for Noise Reduction Using Moving Overlapped Grid Method," Presented at the American Helicopter Society 61st Forum, Grapevine, TX, June 1–3, 2005.

24. JanakiRam, R. D., Sim, B. W., Kitaplioglu, C., and Straub, F. K., "Blade-Vortex Interaction Noise Characteristics of a Full-Scale Active Flap Rotor," Presented at the American Helicopter Society 65th Annual Forum, Grapevine, Texas, May 27-29, 2009.

25. Malovrh, B., and Ghandi, F., "Localized Individual Blade Root Pitch Control for Helicopter Blade-Vortex Interaction Noise Reduction," Journal of the American Helicopter Society, 55, 032007 (2010).

26. Kube, R., van der Wall, B. G., Schultz, K.-J., and Splettstoesser, W. R., "IBC Effects on BVI Noise and Vibrations: A Combined Numerical and Experimental Investigation," American Helicopter Society 55th Annual Forum, Montreal, Canada, May 25-27, 1999.

27. Splettstoesser, W. R., Schultz, K. J., van der Wall, B., Buchholz, H., Gembler, W., and Niesl, G., "Helicopter Noise Reduction by Individual Blade Control (IBC)-Selected Flight Test and Simulation Results," Presented at the RTA – AVT Symposium, Braunschweig, Germany, 8 – 12 May 2000.

28. Potsdam, M., Yeo, H., Johnson, W., "Rotor Airloads Prediction Using Loose Aerodynamic/Structural Coupling," Journal of Aircraft, Vol. 43, No. 3, May–June 2006, pp. 732–742.

29. Lim, J. W., and Strawn, R. C., "Prediction of HART II Rotor BVI Loading and Wake System Using CFD/CSD Loose Coupling," AIAA-2007-1281, Presented at The 45th AIAA Aerospace Sciences Meeting and Exhibit, Reno, Nevada, 8-11 January, 2007.

30. Sim, B. W., and Lim, J., W., "Blade-Vortex Interaction (BVI) Noise and Airload Prediction Using Loose Aerodynamic/Structural Coupling," Presented at the American Helicopter Society 62nd Annual Forum, Phoenix, Arizona, May 9–11, 2006.

31. Lim, J. W., Nygaard, T. A., Strawn, R., and Potsdam, M., "Blade-Vortex Interaction Airloads Prediction Using Coupled Computational Fluid and Structural Dynamics," Journal of the American Helicopter Society, Vol. 52 (4), July 1993, pp. 318–328.

32. Boyd, D. D. Jr., "HART II Acoustic Predictions using a Coupled CFD/CSD Method," Presented at the American Helicopter Society 65th Annual Forum, Grapevine, Texas, May 27–29, 2009.

33. Boyd, D. D., Jr., "Initial Aerodynamic and Acoustic Study of an Active Twist Rotor Using a Loosely Coupled CFD/CSD Method," Presented at The 35th European Rotorcraft Forum, Hamburg, Germany, September 22–25, 2009.

34. Wilbur, M. L., Mirick, P. H., Yeager, Jr., W. T., Langston, C. W., Cesnik, C. E. S., and Shin, S, "Vibratory Loads Reduction Testing of the NASA/Army/MIT Active Twist Rotor," Journal of the American Helicopter Society, Vol. 47 (2), April 2002, pp. 123–133.

35. Fogarty, D. E., Wilbur, M. L., Sekula, M. K., and Boyd Jr., D. D., "Prediction of BVI Noise for an Active Twist Rotor using a Loosely Coupled CFD/CSD Method and Comparison to Experimental Data," Presented at the American Helicopter Society 68th Annual Forum, Forth Worth, TX, May 1-3, 2012.

36. Nichols, R. H., Tramel, R. W., and Buning, P. G., "Solver and Turbulence Model Upgrades to OVERFLOW2 for Unsteady and High Speed Applications," AIAA-2006-2824, Presented at The 36th AIAA Fluid Dynamics Conference, San Francisco, CA, June 2006.

37. Meakin, R. L., "Object X-rays for cutting holes in composite overset structured grids," AIAA-2001-2537, Presented at 15th AIAA Computational Fluid Dynamics Conference, 11-14 June 2001, Anaheim, CA.

38. Johnson, W., CAMRAD II, Comprehensive Analytical Model of Rotorcraft Aerodynamics and

Dynamics, Johnson Aeronautics, Palo Alto, California, 1994.

39. Wilkie, W. K., Wilbur, M. L., and Mirick, P. H., “Aeroelastic Analysis of The NASA/Army/MIT Active Twist Rotor,” American Helicopter Society 55th Annual Forum, Montreal, Canada, May 25-27, 1999.

40. Brentner, K.S.: “Prediction of Helicopter Discrete Frequency Noise – A Computer Program Incorporating Realistic Blade Motions and Advanced Acoustic Formulation,” NASA TM 87721, October 1986.

41. Hennes, C., Lopes, L., Shirey, J., Erwin, J.: “PSU-WOPWOP 3.3 User’s Guide,” The Pennsylvania State University, June 28, 2007.